

March 2020

Monitoring CO₂ underground storage with the Riccati equation

Cand. Real. Knut Sørsdal

Norway, 2020

Abstract

A study is made of an inversion technique of the Riccati type applied to a CO₂-plume on the Sleipner field in the North sea. This paper employs Q-models to introduce forward and inverse filtering of the data. The solution of the Riccati equation with the the Kolsky-Wang Q-model has been presented in previous papers and is applied here. The linear solution of the wave equation introducing attenuation and dispersion has been studied by Wang. He used a modification of Kolsky's Q-model and applied it on a downward continuation algorithm. I have taken the theory further with a general Q-model and a more elegant inversion. The theory is applied on real seismic data from the Sleipner field.

The background model

Higher amounts of CO₂ in the atmosphere has contributed to finding techniques to mitigate the emissions of CO₂. One of those techniques is Carbon Capture and Storage (CCS). CO₂ can be stored in subsurface reservoirs over time. Monitoring and modeling of reservoirs is important to avoid leakage and to predict how the CO₂ could migrate. Modeling is also useful when the seismic interpreter needs a close look at the subsurface data. Then seismic from modeling with known parameters can be useful. I have used the Riccati-equation both for modeling and for inversion to recover the original data used in the seismic theory.

I will connect my theory to real data, and the first place in the world to inject CO₂ was at the Sleipner field in the Norwegian North Sea. The injection found place in 1996 in the Sleipner East field into the Utsira formation. The reservoir is estimated to have a vertical thickness about 200 m at the injection point, and the estimated caprock for the CO₂ is about 100 m thick.

So, this article shows modeling of the seismic response from different synthetic models associated with CO₂ underground storage where the parameters are based on real data.

CO₂ saturation, geometry of the models and some other things are all important parameters affecting the seismic result. I have done calculations with a background model that is saturated with CO₂ and received different results depending on some simple parameters.

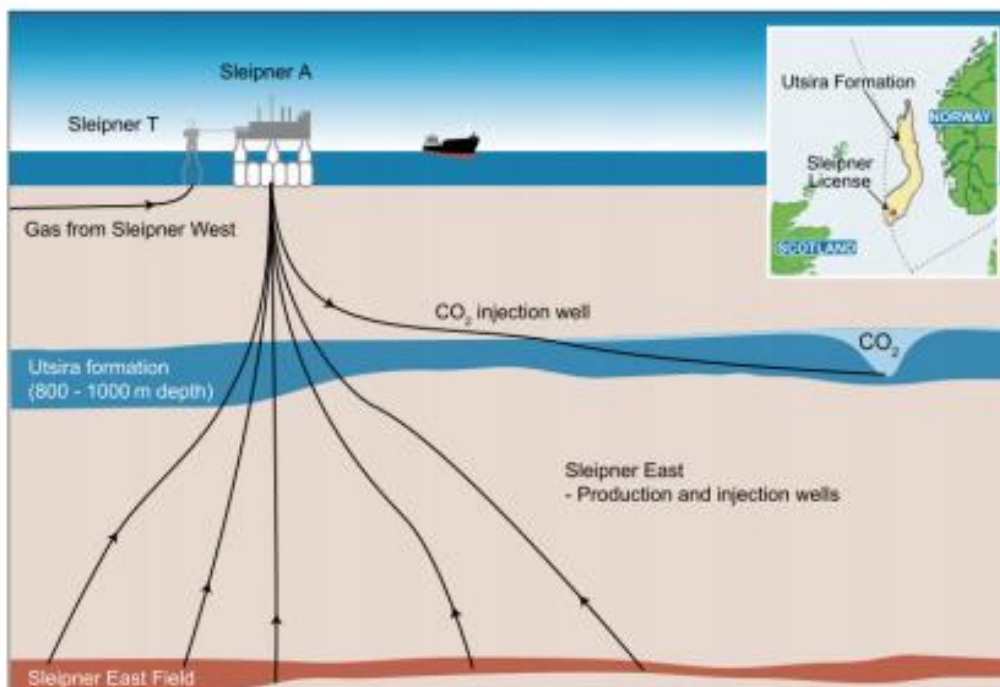


Figure 1. Utsira formation (from IPCC 2005)

Introduction to seismic

Seismic inverse Q-filtering (IQF) is one sector of regular inversion technics that employs a wave propagation reversal procedure that compensates for energy absorption and corrects wavelet distortion due to velocity dispersion. When modelling for the inversion we introduce forward Q-filtering (FQF) models, and will give a short description of the background for such models.

Actually, there is a wide range of mathematical definitions of the Q-model presented in the literature, and Wang (2008) summed up about this. A good start is the Kolsky (1953) model that is used extensively in Q-filtering. Wang proposed to modify the Kolsky's basic attenuation-dispersion model. This was primary an attempt to accurately represent the velocity dispersion effect within the seismic frequency band.

Wang writes that if one compares the basic Kolsky model with other different mathematical Q models, one finds that different models were not close to the basic Kolsky model. Wang, by using a modified Kolsky model, was able to derive a set of analytically derived parameters. The primary goal was to make Kolsky's model comparative with a model satisfying a dispersion condition that is necessary to preserve the causality of a propagating wavelet. Such a dispersion relation is called the Kramers-Krönig dispersion relation. A model of this kind has been discussed by Futterman (1962).

I will use both these Q-models in this article. However, to avoid a rather complicated inverse theory, I will use a least square (LSQ) solution in the Riccati inversion to replace Wang's inverse Q-filtering theory with downward continuation. An attempt with this inversion method without the LSQ-solution was done by Gjevik et al. (1975). In another article Nilsen and Gjevik (1978) presented the theory in a broader way and one absorption model was included. Their theory has been further developed and was presented in the two papers on Researchgate mentioned above.

We will briefly recapitulate their theory by introducing a general absorption model in a forward modelling approach. From this general model we will end up with Q-models of which one will be used in modelling for the inversion as was done in a previous paper, Sørdsdal (2019).

Basics of modelling with absorption included

Inverse Q-filtering algorithms are mainly based on forward wave propagation migration type approach. Then the decay of the frequency content due to absorption can be inspected at each time sample. (Wang (2008).) Following Gjevik we can assume monochromatic plane-waves propagating along a vertical axis. Let P define the stress (pressure) and W the displacement. Density is ρ . Newton's second law gives:

$$\frac{dP}{dz} + \rho\omega^2 W = 0 \quad (1)$$

Correspondingly, a stress-strain relationship of the following form is assumed (Hook's law):

$$P = \rho v_r^2 Y \frac{dW}{dz} \quad (2)$$

In Eq.(2) v_r is the reference velocity which could be taken as the group velocity in case of dispersion. The function Y represents depth and frequency-dependent absorption.

In case of no damping, $Y=1$ and Eq.(2) is simply Hookes law.

Combination of Eqs.(1) and (2.b) gives Helmholtz equation (assume constant density)

$$\frac{d^2 P}{dz^2} + k^2 P = 0, k = \frac{\omega}{v_r \sqrt{Y}} \quad (3)$$

To achieve a complex damping function we can follow Horton (1959) and introduce the notation

$$Y(\omega, \tau) = A(\omega, \tau) + iB(\omega, \tau) \quad (4)$$

In his paper, Horton gives examples of values of A and B for various absorption models that can be causal or non-causal. Since the wavenumber k is in focus, the following expression is now elaborated on

$$\frac{1}{\sqrt{Y}} = \frac{1}{\sqrt{A+iB}} = \frac{\sqrt{A-iB}}{\sqrt{A^2+B^2}} = \frac{(A^2+B^2)^{1/4} [\cos(u/2) - i \sin(u/2)]}{(A^2+B^2)^{1/2}} = \frac{[\cos(u/2) - i \sin(u/2)]}{(A^2+B^2)^{1/4}}$$

$$\tan(u) = \frac{B}{A} \quad (5)$$

Moreover, the following trigonometric relations are valid

$$\tan(u) = \frac{\sin(u)}{\cos(u)} = \frac{\sin(u)}{\sqrt{1-\sin^2(u)}} = \frac{\sqrt{1-\cos^2(u)}}{\cos(u)} = \frac{B}{A} \Rightarrow \quad (6)$$

$$\cos(u) = \frac{A}{\sqrt{A^2+B^2}}, \quad \sin(u) = \frac{B}{\sqrt{A^2+B^2}}$$

And also these

$$\cos(u/2) = \sqrt{\frac{1+\cos(u)}{2}}, \quad \sin(u/2) = \sqrt{\frac{1-\cos(u)}{2}} \quad (7)$$

Finally, combination of Eqs. (5)-(7) gives the result

$$k = \frac{\omega}{v_r \sqrt{Y}} = \frac{\omega}{v_r \sqrt{A+iB}} = \frac{\omega}{v_r} \left[\frac{1}{\sqrt{A}} - \frac{i}{2} \frac{B}{A\sqrt{A}} \right] \quad (8)$$

Now we will compare the real and imaginary part of k for the Q-models. The real part can be related to the phase velocity and the imaginary part is the attenuation coefficient. Then we have: $k_{real} = \frac{\omega}{v_r} \frac{1}{\sqrt{A}}$

$$\text{and } k_{imag} = \frac{1}{2} \frac{\omega}{v_r} \frac{B}{A\sqrt{A}} \quad (9)$$

This leads up to different functions A and B that was calculated in Sørdsdal (2019) and can be related to Q-models. The outline is also given in appendix 1 and is listed in table 1.

		Kolsky Wang (FQF)	
		A	B
1	Kolsky - Wang	$\left[\frac{\omega}{\omega_h}\right]^{2\gamma} \gamma = \frac{1}{\pi Q}$	$\left[\frac{\omega}{\omega_h}\right]^{2\gamma} \frac{1}{Q}$

Table 1.

Fig.3. shows \sqrt{A} (which gives us a hint about the dispersion) for Kolsky-Wang. (Multiplying \sqrt{A} with the reference velocity v_r gives us the phase velocity). According to Kolsky, the tuning frequency ω_h should be the smallest frequency in the frequency band and we use $2\pi\omega_h = 1$ Hz (which obviously is the smallest frequency). This is the red graph on fig.3. Wang modified the Kolsky model by choosing the highest frequency in the frequency band. And that will be the Nyquist frequency $2\pi\omega_h = 125$ Hz (blue graph).

We used the value $Q=200$ and the attenuation coefficient increase linear with frequency (Fig.2). An important aspect with the Kolsky model is that the attenuation will be strictly linear with frequency over the range of measurement.

From fig.3. we can readily see the limitations of the Kolsky model in this context. The red graph shows a phase velocity increasing above the limit 1 (or the reference phase velocity). This was discussed in a previous article (Sørdsdal 2019). This will lead up to a non-causal solution when we use the Q -model in the wave equation since some velocity components will run faster than the reference velocity. That is impossible in physics.

Wang's modification of Kolsky using the Nyquist frequency as tuning (blue graph), gives a phase velocity lower than the reference velocity for the frequency band. This will give a causal solution.

Attenuation coefficient

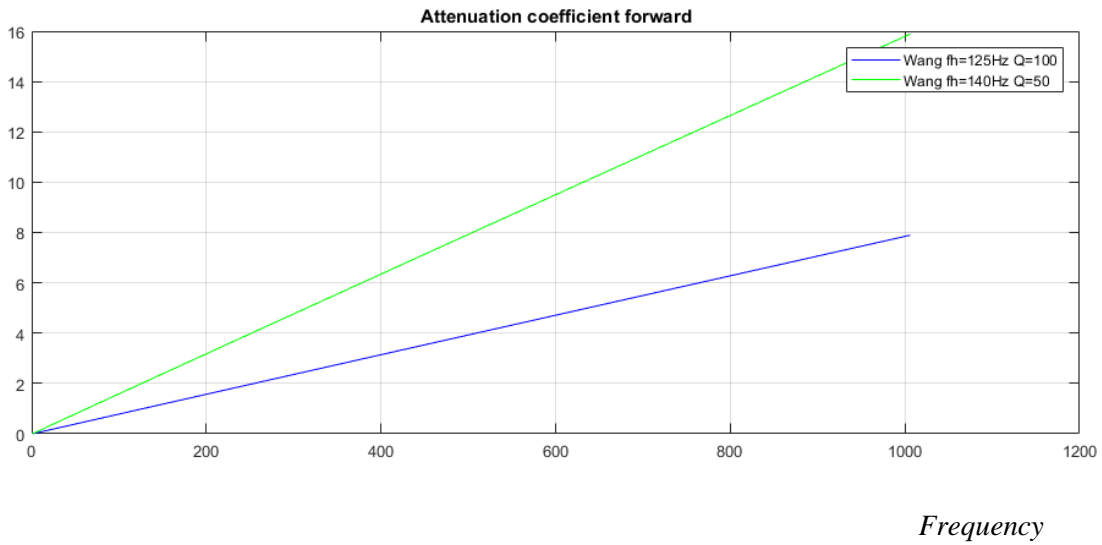


Fig.2. Attenuation coefficient. Attenuation coefficient is dimensioned pr. km or pr.sec.

Phase velocity

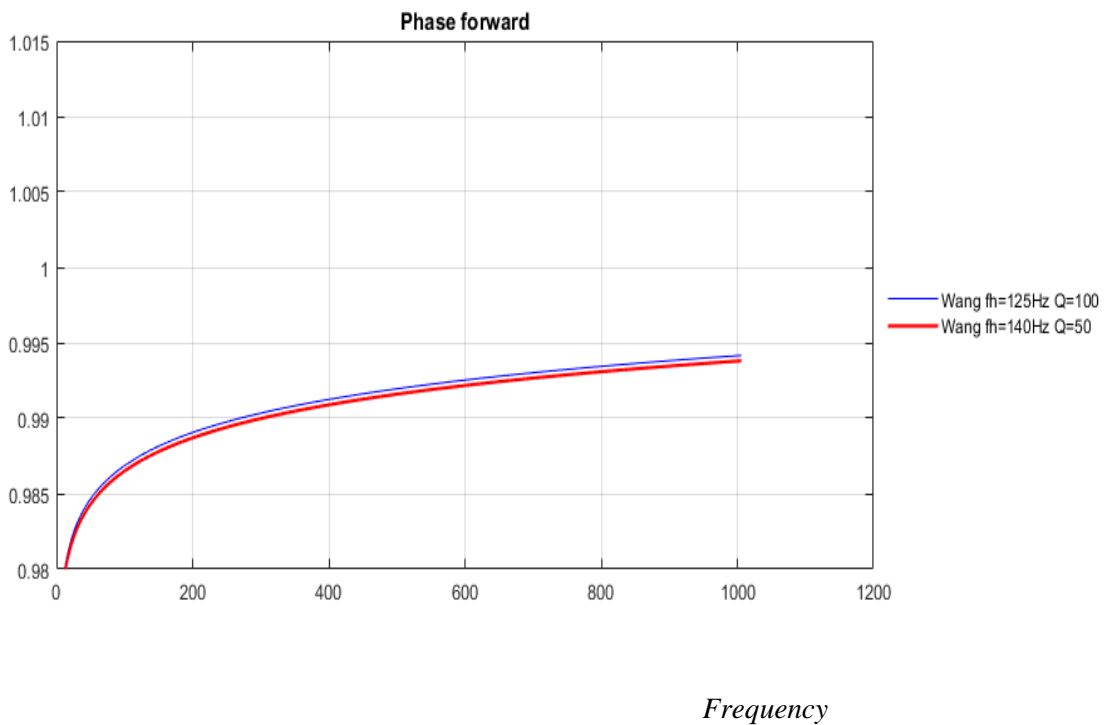


Fig.3. Phase velocity and attenuation coefficient for forward Q -models of table 1. We have used $Q=100$. Wang fh=125Hz (blue) Wang fh=1Hz (red), $Q=50$, fh=140 (green). Phase velocity is dimensionless.

Now we have a forward Q-filters (FQF), of which the absorption model in table 1 in a form modified by Wang could be convenient to use.

Wang (2008) showed that the inverse of FQF for our absorption model, can be calculated simply by changing sign in the exponential for A and B. What is important to realize, however, is that calculations of IQFs for the different FQFs can be complicated when applied to solutions of the wave equation. A more simple solution can be achieved using FQF for the model and solve the inversion with least square filtering (LSQ).

In the following I will show how FQF and LSQ can be implemented in a non-linear solution of the wave equation (the Riccati equation) and apply the solution on the CO2-plume on the Sleipner field .

Introducing the Riccati equation with absorption

The basic idea in a downward wave propagation migration approach is that the wavefield at the surface of the seismic earth model is extrapolated down to a depth z . The real part of k in Eq. (9) describes all dispersion effects during wave propagation and the imaginary part describes absorption.

From Nilsen and Gjevik (1978) we have the Riccati equation:

$$\frac{dK}{dz} = \frac{2i\omega}{v_r \sqrt{Y}} K - r(1 - K^2) \quad (10)$$

K is the complex reflection coefficient and r is the depth-dependent ‘reflectivity’ per depth unity:

$$r(\tau) = \frac{1}{2\rho v_r} \frac{d(\rho v_r)}{d\tau} \quad (11)$$

Since vertically travelling waves are considered, the transformation from depth to two-way travelttime is straightforward

$$\tau = 2 \int_0^z \frac{dz}{v_r}, \Rightarrow d\tau = \frac{2}{v_r} dz \quad (12)$$

Which gives the travel time version of Eq.(10)

$$\frac{dK(\omega, \tau)}{d\tau} = \frac{i\omega}{\sqrt{Y(\omega, \tau)}} K(\omega, \tau) - r(\tau)(1 - K^2), r(\tau) = \frac{1}{2\rho v_r} \frac{d(\rho v_r)}{d\tau} \quad (13)$$

By noticing that

$\exp(-i\omega \int_0^\tau Y(\omega, \tau))^{-1/2} d\tau \equiv \exp[-\phi(\omega, \tau)]$ is an integrating factor for this Riccati equation, it can

be rewritten on the following form:

$$\frac{d}{d\tau} [K(\omega, \tau) \exp(-\phi(\omega, \tau))] = -r(\tau)(1 - K^2) \exp(-\phi(\omega, \tau)) \quad (14)$$

Where

$$\phi(\omega, \tau) = i\omega \int_0^\tau \frac{d\tau}{\sqrt{Y(\omega, \tau)}} = i\omega \int_0^\tau \left[\frac{1}{\sqrt{A}} - \frac{iB}{2A\sqrt{A}} \right] d\tau = \int_0^\tau \left[\frac{i\omega}{\sqrt{A}} + \frac{\omega B}{2A\sqrt{A}} \right] d\tau \quad (15)$$

Assume now the following boundary condition: $K=0$ when $\tau \geq T$. Integration of Eq. (14) now gives the solution

$$-K(\omega, \tau) \exp(-\phi(\omega, \tau)) = -\int_\tau^T r(\tau') \exp(-\phi(\omega, \tau')) (1 - K^2(\omega, \tau')) d\tau' \quad (16)$$

From Eq.(16) we can, when $K^2 \ll 0$, obtain the non-linear solution

$$K(\omega, \tau) = \exp(\phi(\omega, \tau)) \int_\tau^T r(\tau') \exp(-\phi(\omega, \tau')) (1 - K^2(\omega, \tau')) d\tau' \quad (17)$$

Equation (17) is now the starting point for a non-linear modelling algorithm. Assume a discretization in τ (sample interval $\Delta\tau$ and total of N points), and then start at maximum time $T=(N-1)\Delta\tau$ and then calculate K in upward direction.

We introduce the following notation for convenience

$$\begin{aligned} K_{i,j}^n &= K^n(\omega_i, \tau_j) \quad \tau_j = (j-1)\Delta\tau, \quad j = N-1, N-2, \dots, 1 \\ K_{i,N}^n &= 0 \end{aligned} \quad (18)$$

Where the superscript n implies iteration number.

Next, define (trapezoidal rule applied to integral in Eq.(17)) (assume $(n+1)$ th. iteration)

$$\begin{aligned} \beta_{i,j} &= \frac{\Delta\tau}{2} \left[r_{j+1} X_{i,j+1} \{1 - (K_{i,j+1}^n)^2\} + r_j X_{i,j} \{1 - (K_{i,j}^n)^2\} \right], \quad j = N-1, N-2, \dots, 1 \\ r_N &= 0 \end{aligned} \quad (19)$$

Which gives the after sought solution

$$K_{i,j}^{n+1} = \beta_{i,j} / X_{i,j}, \quad j = N-1, N-2, \dots, 1 \quad (20)$$

In Eqs.(18 and 19) we have introduced the operator

$$X_{i,j} = \exp[-\phi(\omega_i, \tau_j)] \quad \tau_j = (j-1)\Delta\tau \quad (21)$$

The seismogram corresponds to the solution $j=1$. The final result in time is obtained after an inverse FFT.

Let the first layer be water, then we need to include the free-surface multiples. Assume that τ_0 represents two-way vertical travel time in the water layer. Total field P_i recorded at the surface (e.g. including multiples) can then be written as (r being the reflection coefficient of the seafloor)

$$P_i = K_{i,j=1} \left[1 - r \exp(-i\omega_i \tau_\omega) + r^2 \exp(-2i\omega_i \tau_\omega) + \dots = \frac{K_{i,j=1}}{1 + r \exp(-i\omega_i \tau_\omega)} \right] \quad (22)$$

Forward numerical implementation

When we make calculations with the models we need to define $r(\tau)$ from a set of layered model parameters connected to the impedance of a seismic media. We can, of course, get r_j from eq (22) as reflectivity per depth unit (1/s). Invoking Eq.(23) we can calculate two-way traveltime by converting the layer thickness z into time and using:

$$r(\tau) = \frac{1}{2(\tau_{j+1} - \tau_j)} \left[\frac{\rho_{j+1} v_{j+1} - 1}{\rho_j v_j} - 1 \right] \quad j=1, \dots, NT-1 \quad (23)$$

We can then get R_j (Reflection coefficients) either by setting ρ and v direct into Eq.(24) or setting r from Eq (23) into Eq.(24). Both r and R are similar physical parameters which represents the contrast in acoustic impedance across an interface. To proceed with computations we must discretize every layer in the model with j and move down to the layer $NT-1$. Velocity and density for each layer we find in table 2.a and b:

$$R_j = \frac{\rho_{j+1} v_{j+1} - \rho_j v_j}{\rho_{j+1} v_{j+1} + \rho_j v_j} = \frac{\exp[2\Delta\tau r_{j+1}] - 1}{\exp[2\Delta\tau r_{j+1}] + 1} \quad \text{for } j = 0, 1, 2, \dots, NT - 1 \quad (24)$$

To set up table 3 for our model parameters we need some data from the Sleipner field. These data we achieved from Nordahl (2015). Data are in table 2. The CO₂-saturation is important when we study the CO₂-layer. Studying fig.4, we were able to set up a model roughly with CO₂-layers 25 m thick and from fig.5 we could locate maximum saturation and put data into table 3. Figure 6 gave us an idea of absorption as a function of CO₂ saturation.

CO ₂ saturation	P-velocity (m/s)
20 %	1568
50 %	1470
100 %	1437

Density (kg/m ³)	Acoustic impedance (Vp·ρ)
2030	$Z_2 = 3,183 \cdot 10^6$
2006	$Z_2 = 2,949 \cdot 10^6$
1965	$Z_2 = 2,824 \cdot 10^6$

Table 2. CO₂ saturation, velocity, density and impedance from Nordahl (2015).

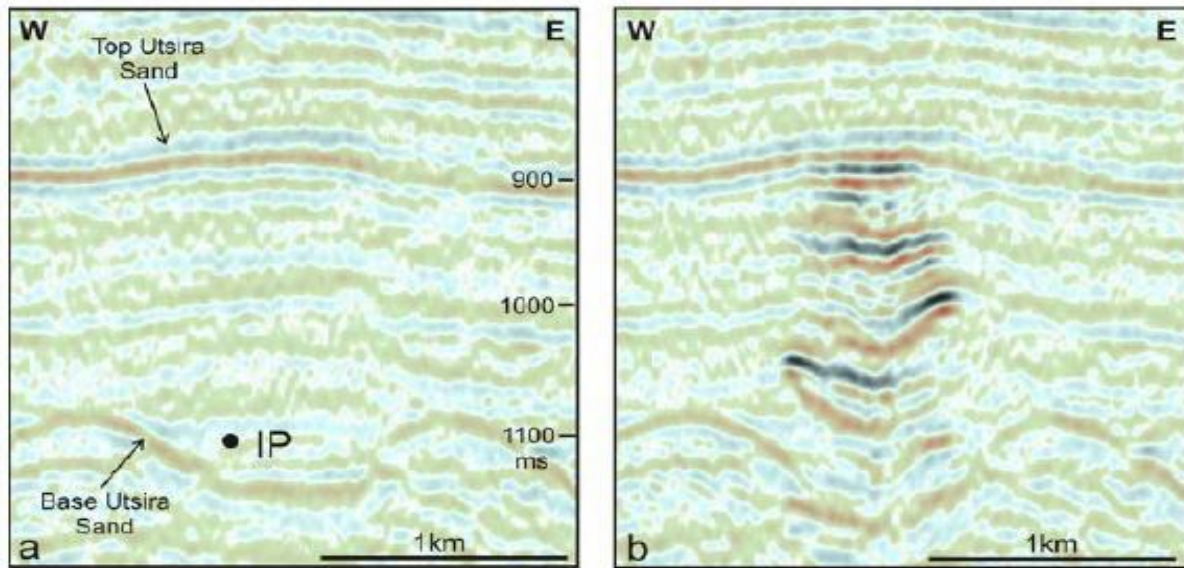


Fig.4. CO2 layers from Utsira sand, Sleipner field

Q	(Depth) Layers	Density ρ g/cm ³	Bgr. dens.	Velocity v km/h	Backgr. velocity	Saturation CO ₂	Depth	Layers
200	80	1.0	1.0	1480	1480		80	Layer 1
200	560	1.5	1.5	1600	1600		640	Layer 2
200	80	2.0	2.0	2500	2000		720	Layer 3 Caprock
100 50	100	1.965 2.03	1.966	1437 1568	2000	100 %	820	Layer 4 CO ₂
50	25	2.03	1.5	1500	1500	25 %	875	Layer 5
200	25	1.96	1.966	1430	1430	25 %	1000	Layer 6

Table 3.. Seismic model parameters

Figure 5 shows data from Sleipner (Hong Yan(2018)). We can see that CO₂-saturation is maximum from 900 m. I will simply use 5 layers in the following calculations, and concentrate on layer 4 (on 875 m) as the CO₂-layer. This layer is expanded up to 100 meters so it will include a section with maximum saturation. Layer 3 is the caprock above the CO₂-plume. We exclude layer 6 in the calculations.

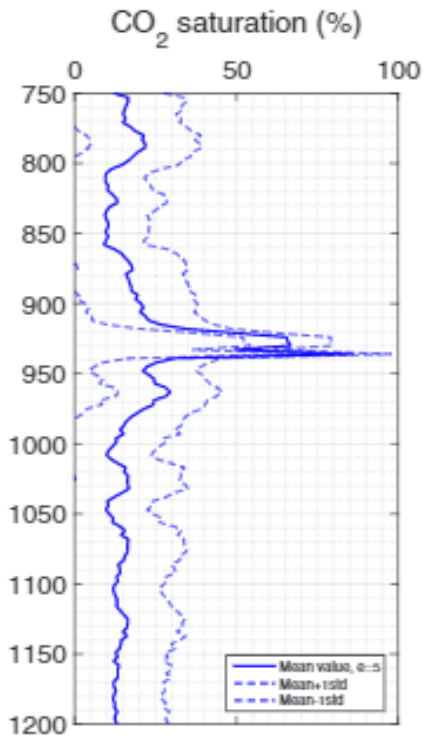


Figure 5. 1D profiles of CO2-saturation estimation taken from Hong Yan (2018). The data is from Utsira sand, Sleipner field. Vertical axes is depth in meters

The CO2-saturation is maximum (estimated 100%) between 900 and 950 meters (marked in table 3).

We also need to take account of the absorption. Fig.6.gives us Q-values for the saturation. We got maximum absorption around 10 %. (Very low Q-values).

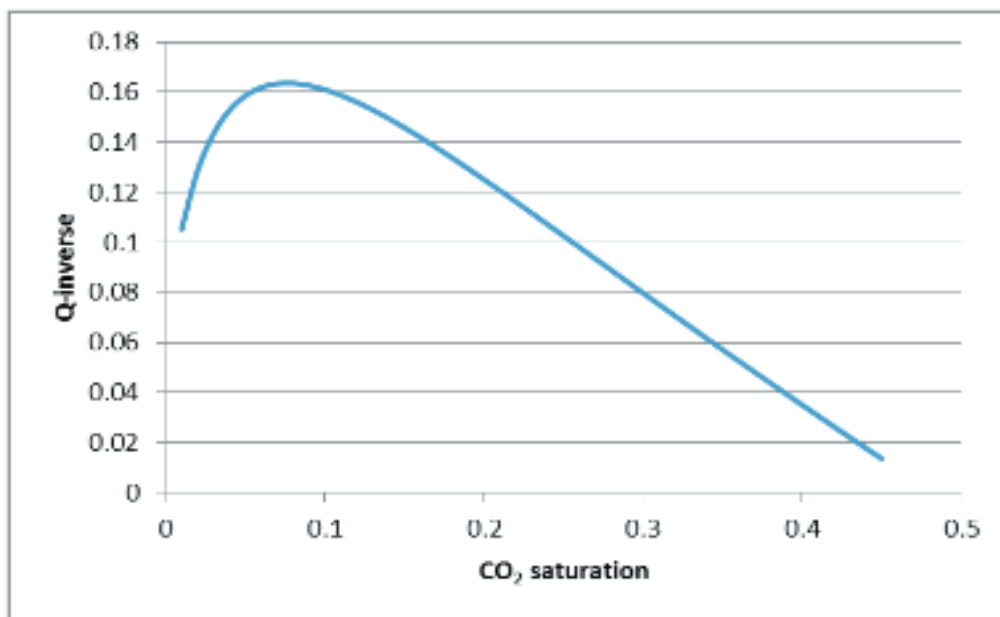


Figure 6 shows data of absorption. Hiroyuki Azuma (2014)

I used some of the data from table 3 for the synthetics. Table 3 is an attempt to include more accurate data for the section taking also the CO2-saturation into account. Synthetics for different shot pulses are on fig.7.

Shot pulse 10 and 30 Hz did not give us visible layers in the Utsira section. Red graph is with attenuation and black graph is undamped. For low frequencies the 30 Hz solution was better than the 10 Hz solution. A shot pulse 60 Hz gave us a better synthetics with all layers visible and attenuated graph (red) is damped compared to undamped (black).

The free-surface-multiples were easily introduced and required a water layer (80m) above the other layers as introduced in Eq.(22). Density of the water layer is 1 g/cm³ and velocity is 1480 km/h. The synthetics with free-surface multiples are graphs to the right on fig.7. With the background model we used Q=200 for attenuation. We have used the absorptionmodel of Wang with $\omega_h=140$ Hz. Other parameters for the background model are from Table 3.

Now, I will set up some alternatives and change the background model for absorption (Q) and velocity (v) in accordance with alternatives in Table 3. This changed model is called the CO2-model. Figure 8 shows solutions for alternative Q values .

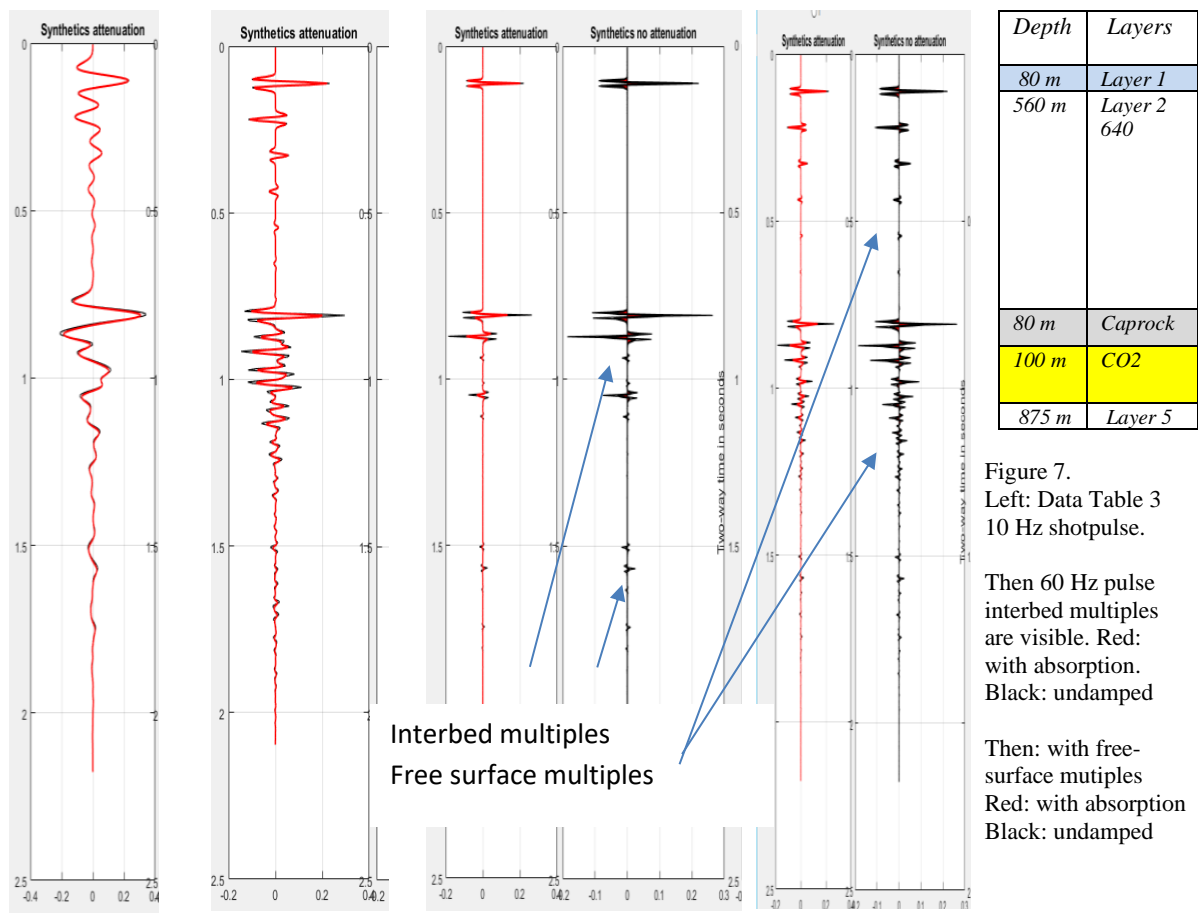
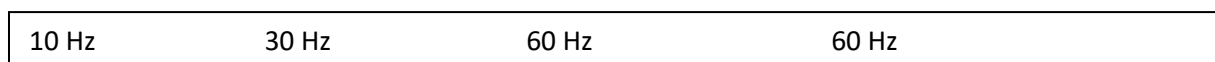


Figure 7. The same data as in figure 7. Layer 2 is changed to Q=100, and next Layer 2 is Q=70 cplot right is both layers Q=100 and Q=70 in same plot.

Q=100 refl.2

Q=70 refl.2

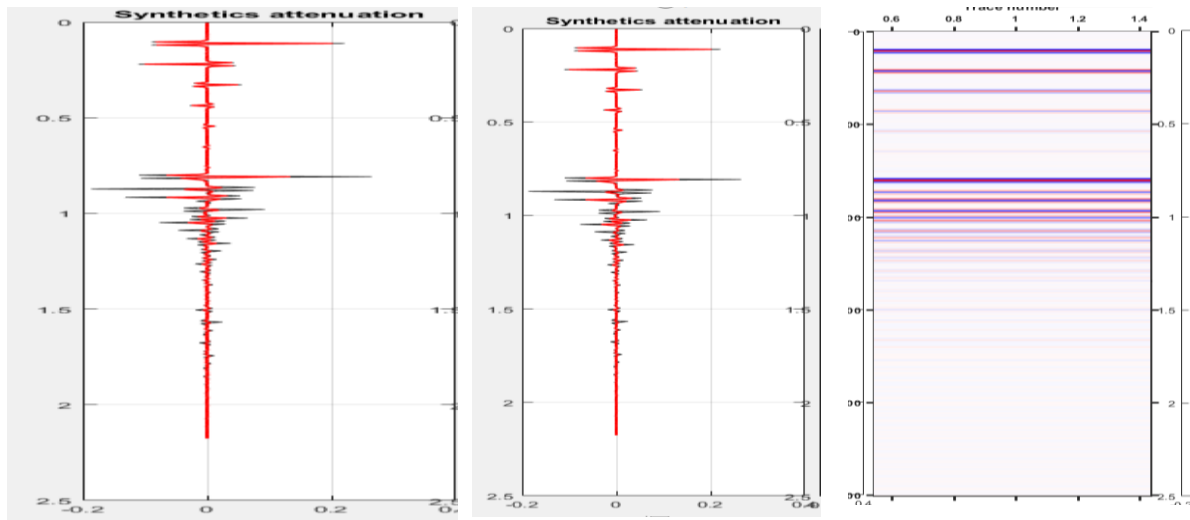


Figure 8. The same data as in figure 7. Layer 2 is changed to Q=100, and next Layer 2 is Q=70 cplot right is both layers Q=100 and Q=70 in the same plot.

Change in velocity will have an effect that is similar to the effect of change in Q-value as long as it gives a less reflector. However, signal from caprock/CO2 will be abruptly changed and can also result in high reflectors. We could expect more interbed multiples.

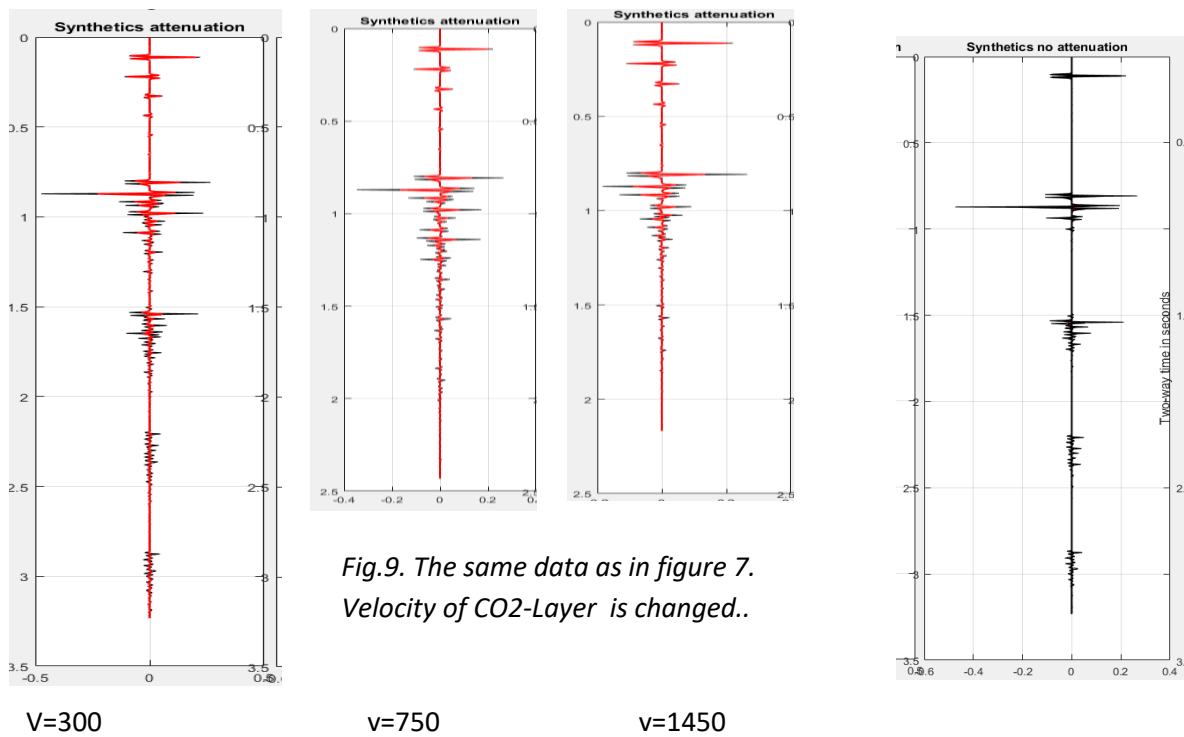


Fig.9. The same data as in figure 7. Velocity of CO2-Layer is changed..

Figure 9 shows that a change in velocity in the CO2 layer will have profound impact on the synthetics below 2.5 seconds. Damped traces (red) do not have so strong effect as undamped. (black).

From fig.7-9 we have a good reconstruction of synthetics with parameters from table 3 and we can conclude that the solution Eq. (17) gives us a good solution of the Riccati-equation in the forward case (synthetics), when the effect of CO2 is taken into account..

Before we jump to the inversion, we need to give a remark about the impedance. The relation between r and the impedance makes it possible to compute the impedance for every solution of r . If the acoustic impedance I_0 is known at $z = 0$, (or at any depth), I is also uniquely determined as a function of τ . From Eq. (11) we can deduce:

$$I = I_0 \exp\left(2 \int_0^{\tau} r(\tau) d\tau\right) \quad (25)$$

where $I_0 = \rho_0 v_0$ and $I = \rho v$. I/I_0 will give us a dimensionless relative impedance. We will come back to this in the next section.

Inverse-Q filtering – inverse numerical implementation

In the following we will implement the layered model parameters (Table 3) that was used to generate the synthetic seismograms in the forward modeling above. The inversion will be done taking the forward modelled synthetic seismograms as input. The procedure will be done with a conventional least square (LSQ) seismic inversion procedure. We will see that an LSQ-inversion is all we need to recover the reflection coefficients from the synthetics .

Consider Eq. (17) in the limit $\tau \rightarrow 0$, which gives the ‘seismogram’

$$K(\omega, 0) = \int_0^T r(\tau') \exp(-\phi(\omega, \tau')) (1 - K^2(\omega, \tau')) d\tau' \quad (26)$$

Introduce ‘reflectivity’ series

$$r(\tau) = \Delta\tau \sum_{i=0}^{NT-1} r_i \delta(\tau - i\Delta\tau), T = NT \cdot \Delta\tau \quad (27)$$

Combination of Eqs. (26) and (27) gives

$$K(\omega, 0) = \sum_{i=0}^{NT-1} r_i \exp(-\phi(\omega, i\Delta\tau)) (1 - K^2(\omega, i\Delta\tau)) \Delta\tau \quad (28)$$

Originally, seismogram recorded in timedomain, i.e. $k(t, 0)$, and assume sampled with a total of NT -samples. Fourier transform of the data will give the same number of monochromatic seismograms.

Nilsen and Gjevik introduced an iterative inversion procedure to solve for r in eq.(26) when the reflection response of the reflecting layer is known. When absorption was included that could be a complicated process and as far as we know no calculations were done with absorption by them.

Leiv Gelius, in an unpublished note, suggested a more elegant solution of the equation with the matrix system:

$$\begin{bmatrix} K_{n+1}(\omega_0, 0) \\ K_{n+1}(\omega_1, 0) \\ \cdot \\ \cdot \\ K_{n+1}(\omega_{NT-1}, 0) \end{bmatrix} = \quad (29)$$

$$\begin{pmatrix} \exp(-\varphi(\omega_0, 0)(1 - K_{0,n}^2) & \exp(-\varphi(\omega_0, \Delta\tau)(1 - K_{1,n}^2) & \dots & \exp(-\varphi(\omega_0, (NT-1)\Delta\tau)(1 - K_{n,n}^2) \\ \exp(-\varphi(\omega_1, 0)(1 - K_{0,n}^2) & \exp(-\varphi(\omega_1, \Delta\tau)(1 - K_{1,n}^2) & \dots & \exp(-\varphi(\omega_1, (NT-1)\Delta\tau)(1 - K_{n,n}^2) \\ \cdot & \cdot & \dots & \cdot \\ \cdot & \cdot & \dots & \cdot \\ \cdot & \cdot & \dots & \cdot \\ \exp(-\varphi(\omega_{NT-1}, 0)(1 - K_{0,n}^2) & \exp(-\varphi(\omega_{NT-1}, \Delta\tau)(1 - K_{1,n}^2) & \dots & \exp(-\varphi(\omega_{NT-1}, (NT-1)\Delta\tau)(1 - K_{n,n}^2) \end{pmatrix} \begin{pmatrix} r_{n,0} \\ r_{n,1} \\ \cdot \\ \cdot \\ r_{n,NT-1} \end{pmatrix}$$

Hagos (2016) made some computations for Eq.(29) in his thesis. A more detailed study of the solution is in appendix 2. The mathematics for how to do least square inversion is also outlined in Sørdsdal (2018).

Note that $K_0^2=0$ in the first iteration. After a new estimate of the reflectivity series has been obtained, an update of $K_{i,n}^2$ can be obtained by solving the forward problem. Iterations are carried out until the relative change in reflectivity is below a certain user threshold. The effect of the inversion when $K^2=0$ is simply to compensate for the damping of the amplitude caused by attenuation and correct the phase term caused by dispersion. When $K^2 \neq 0$ we also remove multiples and compensate transmission loss. Surface multiples can also be removed simply by multiplying K with the inverse of RHS of Eq (22). First we remove surface multiples before we solve Eq.(29). This can simply be done multiplying r with the inverse of Eq. (22)

The solution to Eq.(29) after inversion will be important for further study. The idea of the inversion is to compare the impedance from the seismic model (table 3) with the impedance after the inversion. The success of the inversion depends on how close the impedance we compute from the inverted data are to the impedance from the model data.

Fig.10. a. and b shows a solution r after 5 iterations, and with parameters from table 3 respectively. Surface multiples are removed simply by multiplying r with the inverse of Eq. (22). Then in further iterations interbed multiples are removed so both interbeds and surface multiples are removed in the final solution. (middle graph red).

The impedance-inversion, graph 5 from left, gives a good picture of the inversion. Green graph indistinguishable from black dotted graph shows 5. iteration plotted on the model. The reflectors for the model are on the most right plot. Direct from the reflector we can calculate an impedance we call the reflector-model.

Fig.10.a. gave us a good inversion of the background model removing, interbed multiples and restoring transmission loss. The shot pulse were removed and absorption restored in the final solution.

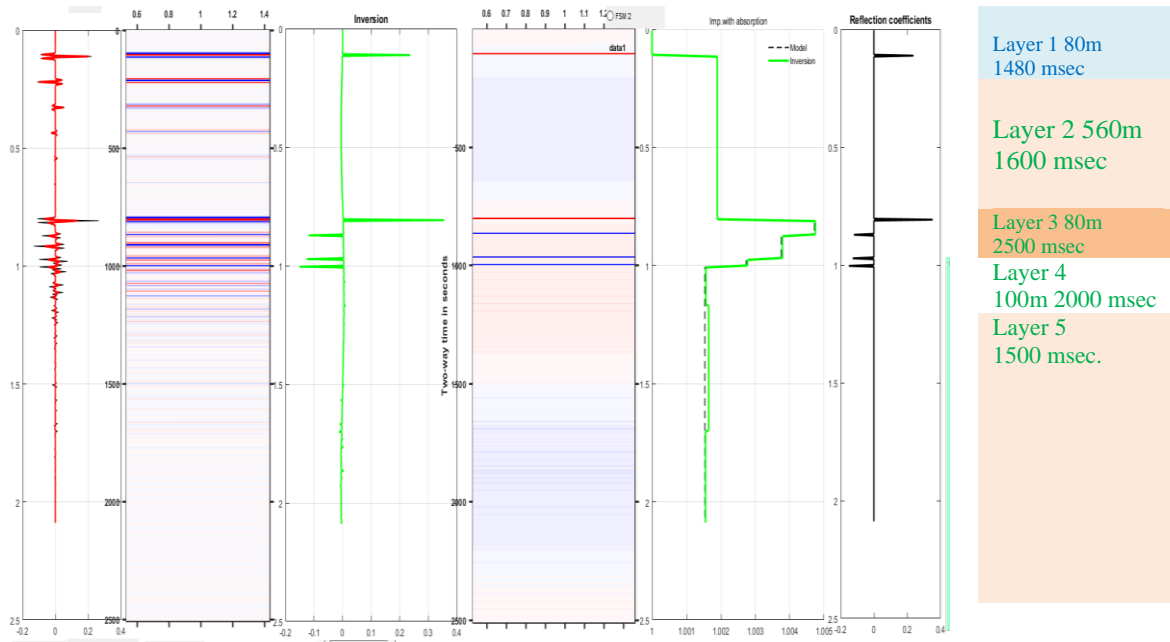


Fig.10.a. Data from table 3. From left: Synthetics with all multiples. Then synthetics cplot. Then full background inversion , and then cplot inversion. Background impedance inversion is close to the model. (black dotted). Right plot: reflection coefficients for the model. $Q=200$.

Now to the CO2-saturated model. CO2 will give lower density and slower velocity. Highly saturated model will give lower attenuation than less saturated (maximum at 10 % CO2 saturation).

Fig.10.b gives an inversion of the saturated model for different parameters. Fig.10.c. deviates from fig.10.b. simply by a change of absorption from $Q=200$ to $Q=100$ in the CO2-layer.

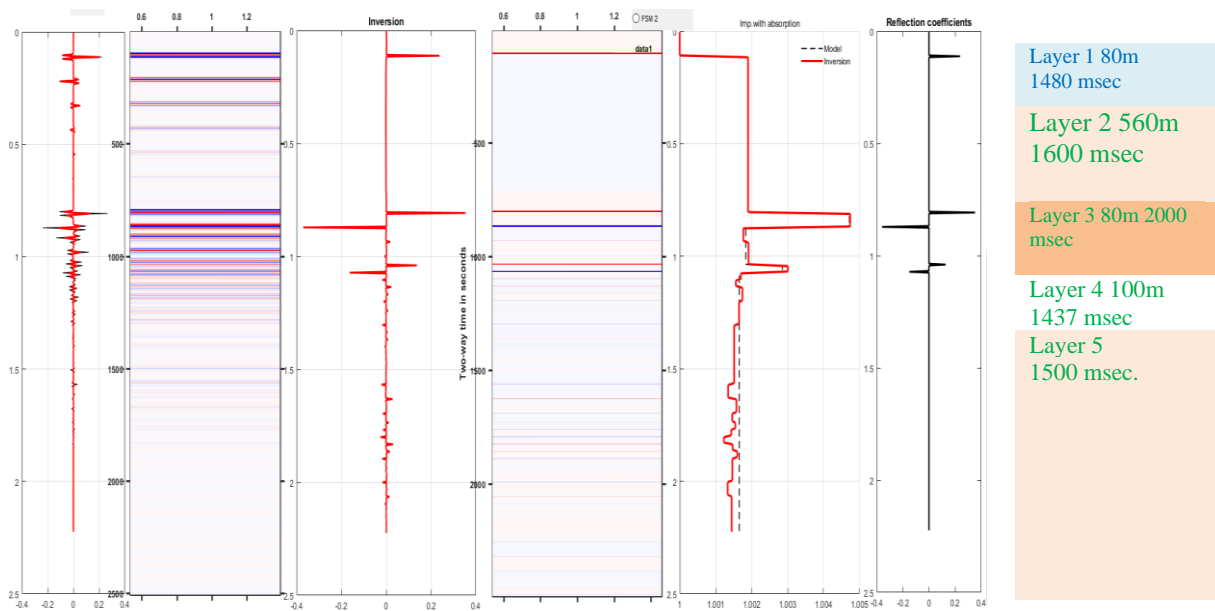


Fig.10.b. Data from table 3 (CO2 saturated). From left: Synthetics with all multiples). Then synthetics cplot. Then full CO2-saturated inversion and then cplot inversion. Then impedance inversion, and Reflector model is to the right. $Q=200$

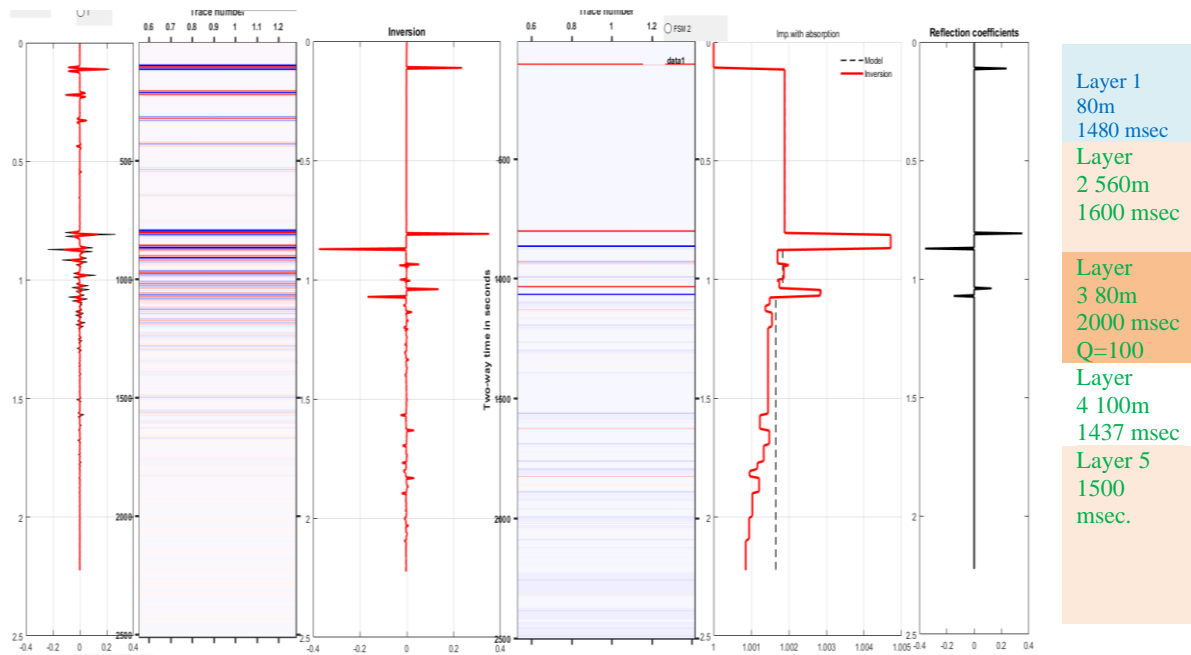


Fig.10c. Data from Fig10.b. Absorption is changed to $Q=100$ in CO2 layer

Fig.10 d. is the background model with data from fig.10 a. (green). Red graph is saturated model from fig.10.b. with a small modification. Velocity through layer 3 is changed from $v=2000$ msec to $v=2500$ msec. The reason for this is that this velocity made the CO2 saturated model more close to the reflector-model. (dotted line).

It is important to notice that the lag between the background model and the CO2-saturated model is due to slower velocity in the saturated model. The absorption will also give some dispersion, but slower velocity will dominate. We will be able to see this, knowing that all dispersion caused by viscoelasticity is corrected for in the LSQ-inversion. I have documented this in previous articles Sørdsdal (2018) and Sørdsdal (2019). The velocity change, however, is not corrected for in the inversion of the saturated model. I will come back to this in a later article.

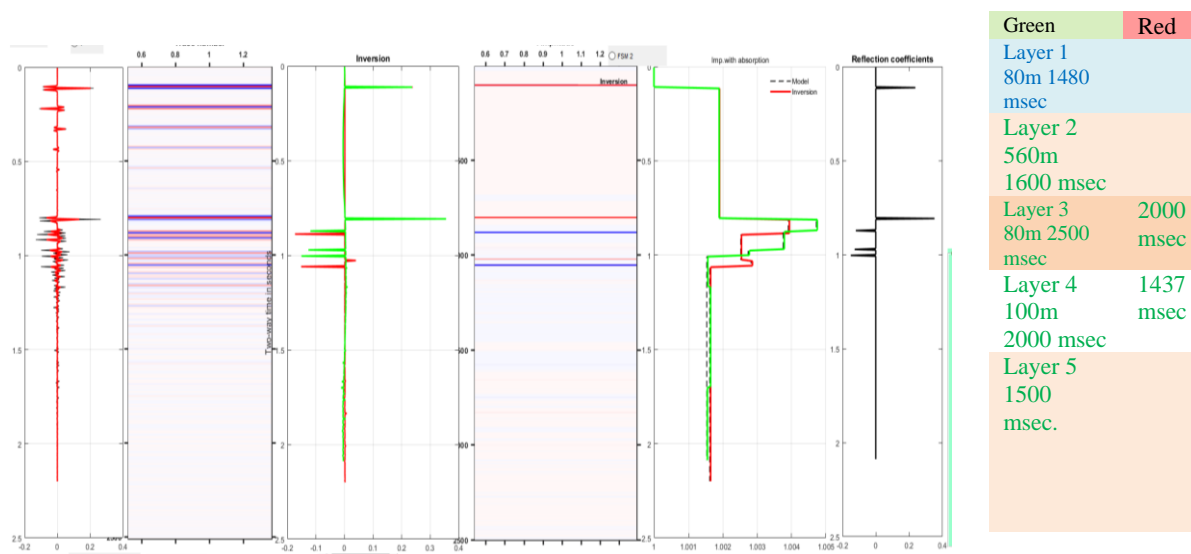


Fig.10d. Impedance inversion, green (left) background model, red (right) CO2-model

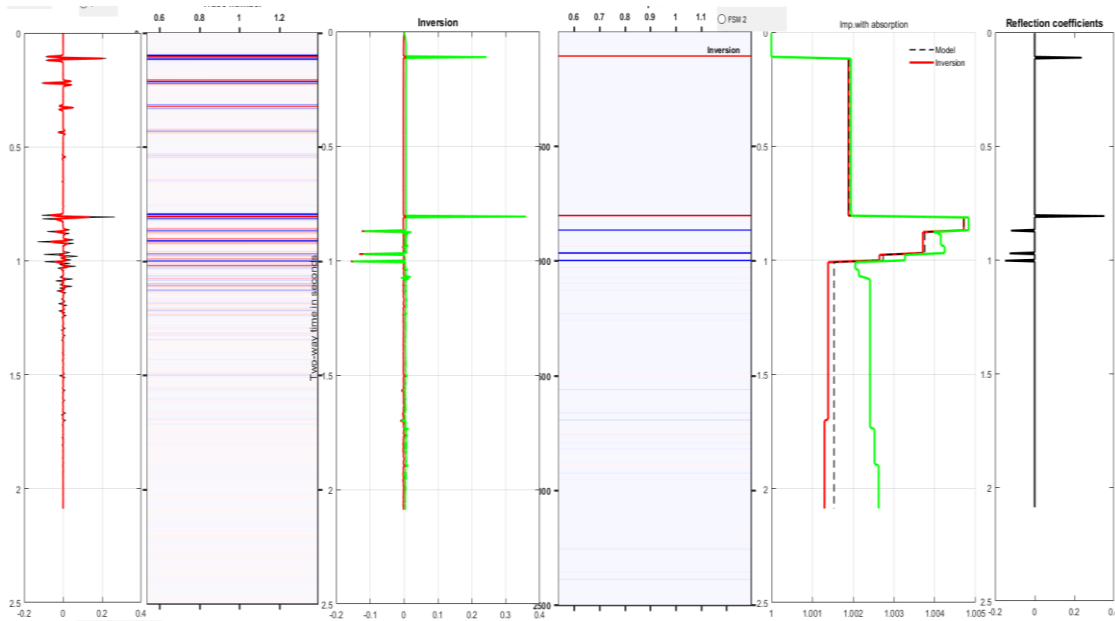


Fig.11.a Impedance inversion green $Q=68$, red $Q=100$ in CO2-layer

Fig.11.a. is close to fig.10.d.but with more absorption ($Q=68$). Left is synthetics with all multiples. Then inversion of CO2-saturated model. We can see layers are a bit disordered for the impedance inversion. C-plot right is inversion of background model. This is very well restored.

On fig.11 b we see saturated CO2 model for different Q-values. Left plot is synthetics with all multiples. Then cplot of synthetics. Next cplot is inversion with $Q=67$. It deviates much from the reflector model, and is of no use.

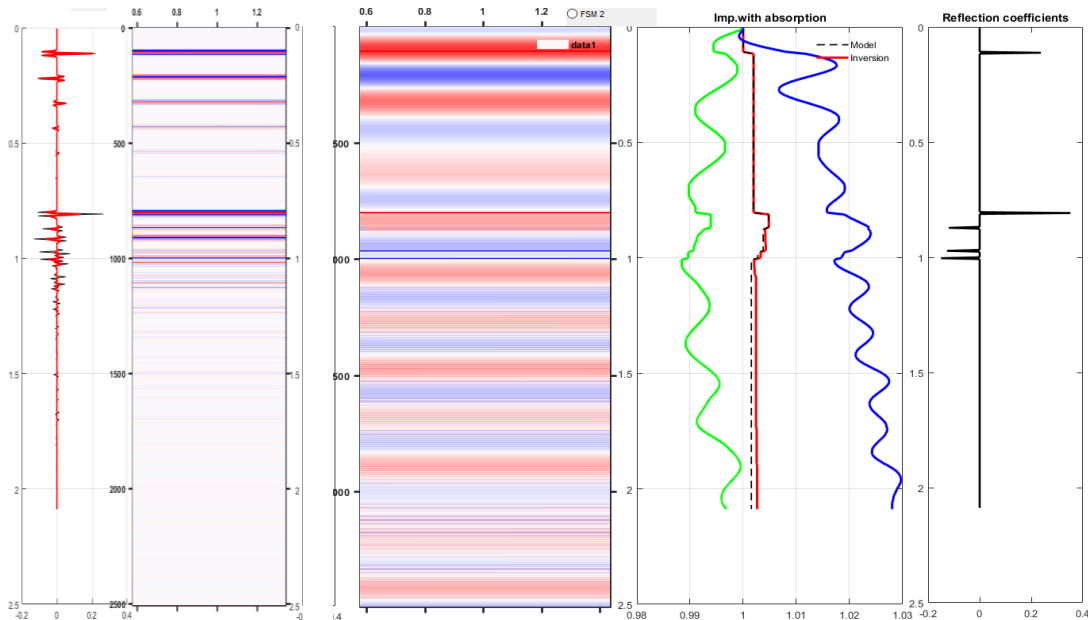


Fig.11.b. Problems with inversion for high absorption green $Q=67$, blue $Q=68$ red $Q=100$.

Fig.11.c gives us the same data as fig.11.b with higher Q-values. However, cplot of the inversion gave us a solution similar to the cplot of fig.11.a. we can conclude that we get a good inversion as long as Q is higher than 68.

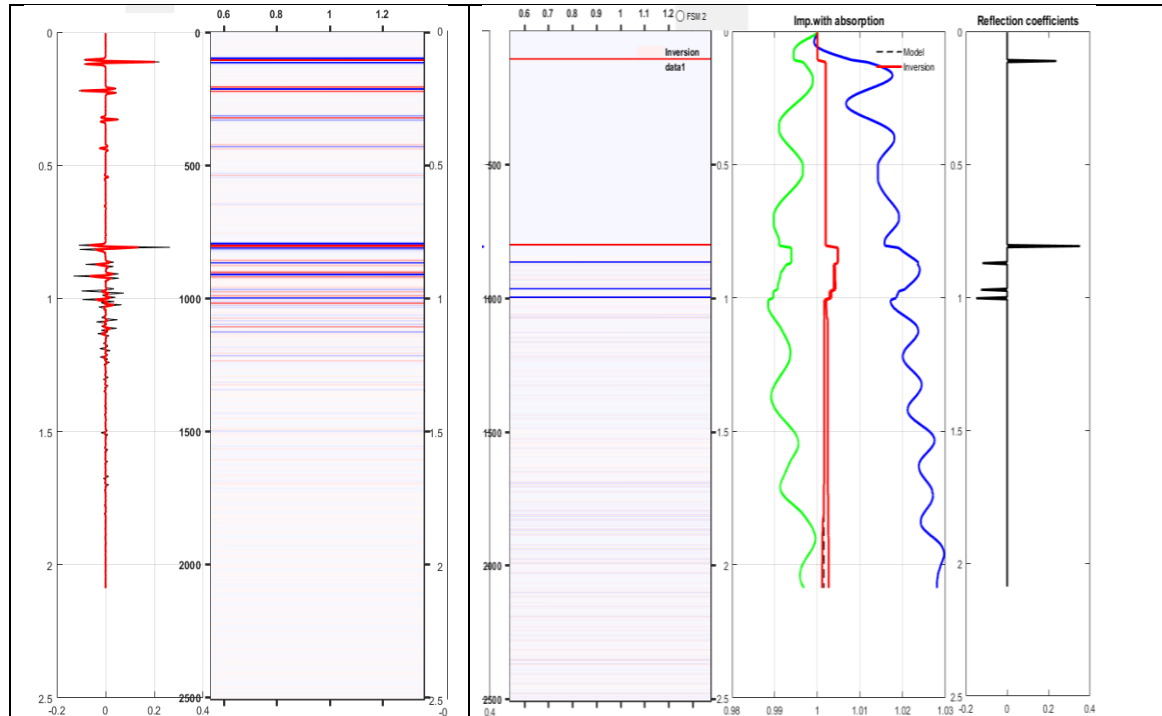


Fig.11.c. Absorption $Q=69$ give a good inversion (red plot) with a cplot (middle plot) similar to fig.11.a.

To sum up, we got a very good solution with LSQ, indistinguishable from the model for our impedance models (Table 3). The inclusion of surface multiples were very good implemented, but not important for our theory, since we removed them before using LSQ. All the other effects, however, are important for the LSQ-solution.

The first and second graph from left for fig.10-11.a, b, c and d represent synthetics as a trace and a c-plot. And all features are introduced by 5 iterations, attenuation and dispersion included.

Then we use synthetics as input counting K^2 zero and computing the first LSQ-solution for K. Now we put this K into Eq. (29). and get a new iterated inversion. We repeat this 5 times. Then we see that interbed multiples are removed and transmission loss and attenuation are restored as well as shot pulse removed. Dispersion is also compensated for. However, attenuation is not so good restored for with $Q < 69$. Fig.11 b and c and shows the calculations with lower Q-values. Impedance inversions shows a solution very different from the background model, and we can expect problems studying inversion with high attenuation.

A closer look at the inversion

Ultimately, after the development of the previous theory we have been able to combine a forward solution of Kolsky-Wang Q-filter with a LSQ-solution for inversion. So we have fulfilled the purpose of this article. However, a broader view of the subject could be interesting in the future and a further study of Q-filtering is necessary. As mentioned above fig.11.b and c shows an impedance inversion far from the background model for higher attenuation.

So, to further sum up: setting $K^2=0$ in eq (29) we achieved the linear solution on matrix form and solved this for r as a time-domain vector that represents the filter. The inverse Q-filtering procedure was performed successively to each time sample to get the time-dominant output vector. We then used the output r as input getting the inverted solution for a new inverted r . When we do this we can, of course, replace the Q-filters with the inverse Q-filters as Wang did, and this could be a further study. Then we also will need to study the stabilization of the inverse filter, gain limitation and so on. However, the LSQ-solution in this paper simplified the study. The stabilization was introduced in another form than with Wang in the LSQ-solution in appendix 2. It is called the regularization of the LSQ-solution. Further iterations introduce non-linearity on the way to a seismic theory that can be used on real data and will be, as far as I can see, a broader and better theory than the theory of Wang that was strictly linear.

Conclusion

The results of the preceding sections show that the Riccati equation with Q-filtering provides a method for the construction of synthetic reflection seismograms that is a continuation of the method introduced by Nilsen and Gjevik. Moreover does this theory describe a method for inverting reflection data, i.e. computing the variations in the acoustic impedance within a reflecting layer that can be used in real prospecting. This I have briefly suggested by introducing a water layer in the seismic model on a very simple seismic model from the Sleipner field. And the Riccati inversion corrects phase, compensates frequency loss, removes multiples and compensates transmission loss in one single process.

In my previous articles I tested the abilities of the inversion method by inverting a synthetic reflection seismograms computed from a simple impedance model with a water layer. And frankly, this article does not introduce so much more that concern real seismic prospecting. It would, however – as Gjevik suggested several years ago - be interesting to apply the present inversion method to real reflection data from a more complex structure. A number of problems will then arise as was discussed in the paper of Nilsen and Gjevik. However, because of years of rapid development in inversion theory, this is much easier solved today than when the theory first was introduced .

Even if this could be done only with a limited degree of accuracy, the main problem is, however, that what Gjevik asked is not fully answered: will one lose so much information or introduce so many errors through this process that the inversion becomes meaningless when applied to real prospecting? In view of the success of the application on data from the Sleipner field this question could soon be answered.

References

- Gjevik et al. (1976) An attempt at the inversion of reflection data. Geophysical prospecting 24,492-505*
Nilsen and Gjevik (1978): Inversion of reflection data. Geophysical prospecting 26, 421-432

Yanghua Wang (2008) Blackwell Publishing. Seismic inverse Q filtering

Knut Sørsdal (1981) Viskoelastiske dempningsmodeller i Riccatiligningen anvendt i marin seismikk. University of Oslo

Knut Sørsdal (2019) Seismic Q-filter models applied to the Riccati equation
https://www.researchgate.net/publication/337682839_Seismic_Q-filter_models_applied_to_the_Riccati_equation

Knut Sørsdal (2018) 1-D non-linear inversion of data with absorption - revisited.
https://www.researchgate.net/publication/331257025_1-D_non-linear_inversion_of_data_with_absorption_-_revisited

Bland(1960) The theory of linear viscoelasticity. Pergamon Press

Horton (1959) A loss mechanism for the Pierre Shale. Geophysics vol.24, no 4

Aki and Richards (2002) Quantitative Seismology W.H. Freeman and Co. San Fransisco

Kolsky, 1956 The propagation of stress pulses in viscoelastic solids. Philosophical Magazine 1, 693-710

Kjartansson E. 1979 Constant Q wave propagation and attenuation. Journal of Geophysical Research 84 4737-48.

Futterman W.I 1962 Dispersive body waves. Journal of Geophysical Research 67 , 5279-91

Trorey A.W, 1962 Theoretical seismograms with frequency and depth dependent absorption. Geophysics 27, 766-85

Claerbout J.F.1976 Fundamentals of Geophysical Data Processing. McGraw-Hill Book Co. New York

Hagos Geberehiwet Gebregergs (2016): Compensation of Absorption Effects in Seismic Data. University of Oslo

Hong Yan, Bastien Dupuy, Anouar Romdhane and Børge Arntsen
Geophysical Prospecting, 2019, 67, 1055–1071 CO₂ saturation estimates at Sleipner (North Sea) from seismic tomography and rock physics inversion

Janita Louise Nordahl : (2015) Modeling of seismic amplitude anomalies associated with CO₂ underground storage — EOM-3901 Master's Thesis in Energy, Climate and Environment

KARSTENS, J. & BERNDT, C. 2015. Seismic chimneys in the Southern Viking Graben – Implications for palaeo fluid migration and overpressure evolution. Earth and Planetary Science Letters, 412, 88-100.

HALLAND, E. K., JOHANSEN, W. T. & RIIS, F. 2011. CO₂ Storage Atlas Norwegian North Sea, Norwegian Petroleum Directorate.

ARTS, R., EIKEN, O., CHADWICK, A., ZWEIGEL, P., VAN DER MEER, B. & KIRBY, G. 2004a. Seismic monitoring at the Sleipner underground CO₂ storage site (North Sea). Geological Society, London, Special Publications, 233, 181-191.

ARTS, R., EIKEN, O., CHADWICK, A., ZWEIGEL, P., VAN DER MEER, L. & ZINSZNER, B. 2004b. *Monitoring of CO2 injected at Sleipner using time-lapse seismic data. Energy, 29, 1383-1392.*

Hiroiyuki Azuma (2014) *Utilization of seismic attenuation in the monitoring of CO2 geological storage project. Science Direct.*

Appendix 1

In the literature the wavenumber k is often written on the following form in case of absorption (constant-Q model)

$$k = \frac{\omega}{v(\omega)} \left[1 - \frac{i}{2Q} \right] = \frac{\omega}{v_r} + \left[\frac{\omega}{v(\omega)} - \frac{\omega}{v_r} \right] - i\alpha(\omega) = \frac{\omega}{v_r} + \varphi(\omega) - i\alpha(\omega). \quad \alpha = \frac{\omega}{2Qv(\omega)} \quad (\text{A.1})$$

Where α is the absorption coefficient and φ is the phase of the ‘absorption filter’. In order to ensure causality, the filter should be minimum phase. For such a filter this relationship holds.

$$\varphi(\omega) = H[\alpha(\omega)]$$

With H denoting the Hilbert Transform. In case of no dispersion ($\varphi=0$), the filter will be noncausal. Then we have

$$k = \frac{\omega}{v_r \sqrt{Y}} = \frac{\omega}{v_r \sqrt{A + iB}} = \frac{\omega}{v_r} \left[\frac{1}{\sqrt{A}} - \frac{i}{2} \frac{B}{A\sqrt{A}} \right] \quad (\text{A.2})$$

Equating Eqs. (A.1) and (A.2) gives the relationships

$$A = \left[\frac{v(\omega)}{v_r} \right]^2 \quad B = \left[\frac{v(\omega)}{v_r} \right]^2 \frac{1}{Q}, \quad (\text{A.3})$$

Aki and Richards (2002) show that the following relation should be held to honor causality

$$\frac{\omega}{v(\omega)} - \frac{\omega}{v_\infty} = H \left[\frac{\omega}{2Qv_\infty} \right] \quad (\text{A.4})$$

Where v_∞ is the limit of the velocity function when ω tends to infinity. Equation (12) can be further approximated as

$$\frac{\omega}{v(\omega)} - \frac{\omega}{v_h} \cong H \left[\frac{\omega}{2Qv_\infty} \right] \quad (\text{A.5})$$

Where v_h is the velocity related to the highest possible (tuning) frequency of the seismic band. The wavenumber is accordingly adjusted as (compare with Eq.(A.1)).

$$k = \frac{\omega}{v_h} + \left[\frac{\omega}{v(\omega)} - \frac{\omega}{v_h} \right] - i \frac{\omega}{2Qv(\omega)} = \frac{\omega}{v_h} \left\{ 1 + \left[\frac{v_h}{v(\omega)} - 1 \right] - i \frac{v_h}{2Qv(\omega)} \right\} \quad (\text{A.6})$$

And combined with a Kolsky type of phase-velocity model (Kolsky, 1956)

$$v(\omega) = v_h \left(\frac{\omega}{\omega_h} \right)^\gamma, \quad \gamma = (\pi Q)^{-1} \quad (\text{A.7})$$

Gives the wavenumber model

$$k = \frac{\omega}{v_h} \left[1 + \left[\left(\frac{\omega}{\omega_h} \right)^{-\gamma} - 1 \right] - \frac{i}{2Q} \left(\frac{\omega}{\omega_h} \right)^{-\gamma} \right] \quad (\text{A.8})$$

Which has been employed by Wang. From Eqs. (A.1) and (A.2) it also follows that ($v_r = v_h$)

$$A_{Wang} = \left[\frac{\omega}{\omega_h} \right]^{2\gamma} B_{Wang} = \left[\frac{\omega}{\omega_h} \right]^{2\gamma} \frac{1}{Q} \quad (\text{A.9})$$

From Eq.(A.9) it follows that $0 < A_{Wang} < 1$, and the same for B_{Wang} but with $B_{Wang} \ll A_{Wang}$.

Based on Eq. (A.3), Kjartansson (1979) proposed an alternative wavenumber model

$$k = \frac{\omega}{v_\infty} + \left[\frac{\omega}{v(\omega)} - \frac{\omega}{v_\infty} \right] - i \frac{\omega}{2Qv_\infty} = \frac{\omega}{v_\infty} + H \left[\frac{\omega}{2Qv_\infty} \right] - i \frac{\omega}{2Qv_\infty} \quad (\text{A.10})$$

From Eqs.(11) and (A.10) it follows that ($v_r = v_\infty$)

$$A_{Futt} = \left[1 + \frac{1}{\omega} H \left(\frac{\omega}{2Q} \right) \right]^{-2} B_{Futt} = (A_{Futt})^{3/2} \frac{1}{Q} \quad (\text{A.11})$$

For completeness, we also have the dispersion-free and non-causal absorption model of Futterman (1962), which corresponds to

$$A_{Futt} = 1 \quad B_{Futt} = \frac{1}{Q} \quad (\text{A.12})$$

Ricker wavelet in the synthetics

In order to get the synthetic seismogram in time domain by inverse Fourier transform of the complex reflection coefficient K , each component of K (Eq.(26) is multiplied by a sampled Ricker wavelet in frequency domain:

$$Srw = (2/\sqrt{\pi}) \frac{f^2}{f_c^3} \exp\left(-\frac{f}{f_c}\right)^2 \quad (\text{A.13})$$

This Ricker wavelet is a zero-phase wavelet and is non-causal. The frequency f_c is called the center frequency and will vary.

Appendix 2

To apply least-square inversion, Eq. (29) can be written in vector and matrix notation in short as

$$\vec{K} = M \vec{r} \quad (\text{A14})$$

where

$$\vec{K} = \begin{bmatrix} K_{n+1}(\omega_0, 0) \\ K_{n+1}(\omega_1, 0) \\ \vdots \\ K_{n+1}(\omega_{NT-1}, 0) \end{bmatrix} \quad \vec{r} = \begin{bmatrix} r_{n,0} \\ r_{n,1} \\ \vdots \\ r_{n,NT-1} \end{bmatrix}$$

$$M = \Delta\tau \begin{bmatrix} \exp(-\varphi(\omega_0, 0)(1 - K_{0,n}^2)) & \exp(-\varphi(\omega_0, \Delta\tau)(1 - K_{1,n}^2)) & \dots & \exp(-\varphi(\omega_0, (NT-1)\Delta\tau)(1 - K_{n,n}^2)) \\ \exp(-\varphi(\omega_1, 0)(1 - K_{0,n}^2)) & \exp(-\varphi(\omega_1, \Delta\tau)(1 - K_{1,n}^2)) & \dots & \exp(-\varphi(\omega_1, (NT-1)\Delta\tau)(1 - K_{n,n}^2)) \\ \vdots & \vdots & \dots & \vdots \\ \vdots & \vdots & \dots & \vdots \\ \exp(-\varphi(\omega_{NT-1}, 0)(1 - K_{0,n}^2)) & \exp(-\varphi(\omega_{NT-1}, \Delta\tau)(1 - K_{1,n}^2)) & \dots & \exp(-\varphi(\omega_{NT-1}, (NT-1)\Delta\tau)(1 - K_{n,n}^2)) \end{bmatrix} \quad (\text{A15})$$

\vec{K} is a (N \times 1) vector, M is a (N \times N) matrix and \vec{r} is a (N \times 1) vector. Let \vec{K} be the desired seismic output data while the actual output from Eq. (A14) is $\vec{S} = M \vec{r}$. We want to compute a reflectivity per depth unit series \vec{r} such that the difference $\vec{\Sigma}$ between the actual output \vec{S} and the predicted seismic output data \vec{K} is minimum in the least square sense. Therefore, the error $\vec{\Sigma}$ with respect to parameter vector \vec{r} is $\vec{\Sigma} = \vec{K} - \vec{S} = \vec{K} - M\vec{r}$. And the cumulative squared error:

$$\vec{\Sigma}^T \vec{\Sigma} = (\vec{K} - M\vec{r})^T * (\vec{K} - M\vec{r}) =$$

$$(\vec{K}^T * \vec{K} - \vec{K}^T M\vec{r}) - r^T M^T K^T + (\vec{r}^T M^T * M\vec{r}) \quad (\text{A16})$$

Where T denotes matrix transpose and * denotes complex conjugate.

We want to estimate a reflectivity per depth unit series \vec{r} such that the quantity $\vec{\Sigma}^T \vec{\Sigma}$ is minimum. This condition leads to setting the derivative of $\vec{\Sigma}^T \vec{\Sigma}$ with respect to \vec{r} to zero. Differentiate both sides of eq. (A16) with respect to \vec{r} and observe the requirement for least square procedure minimization that

$$\frac{\delta \vec{\Sigma}^T \vec{\Sigma}}{\partial \vec{r}} = -\vec{K}^T * M + r^T * M^T * M = 0 \quad (\text{A17})$$

Because \vec{r}^{T*} is complex valued, $\frac{\delta \vec{r}^{T*}}{\delta \vec{r}} = 0$. Thus applying matrix transpose and rearranging the terms of eq. (A17)

$$\begin{aligned} (M^T * M)^T * \vec{r} &= M^T \vec{K} \Rightarrow (M^T M) \vec{r} = M^T * \vec{K} \\ \Rightarrow \vec{r} &= (M^T * M)^{-1} M^T \vec{K} \end{aligned} \quad (\text{A18})$$

Eq (A18) will give us the reflectivity per depth unit and from this we can calculate the impedance.

Damping constant when calculating reflectivity

To further understand the inversion we need to discuss how reflectivity per depth unit is computed and the introduction of the matrix M defined in Eq.(A14). However an important aspect must be discussed first. The singularity of the matrix $M^T * M$ makes it necessary to introduce a damping constant λ when calculating r . This λ is chosen out from the 'singular value decomposition' (svd) of the matrix $M^T * M$. Now we get an invertible new matrix:

$$L = \text{svd}(M^T * M) \text{ giving } M^T * M + \lambda I$$

I is a unitary matrix of the same order as the matrix $M^T * M$

$$\begin{aligned} (M^T * M)^T * \vec{r} &= M^T \vec{K} \Rightarrow (M^T M) \vec{r} = M^T * \vec{K} \\ \Rightarrow \vec{r} &= (M^T * M)^{-1} M^T \vec{K} \end{aligned} \quad (\text{A.19})$$

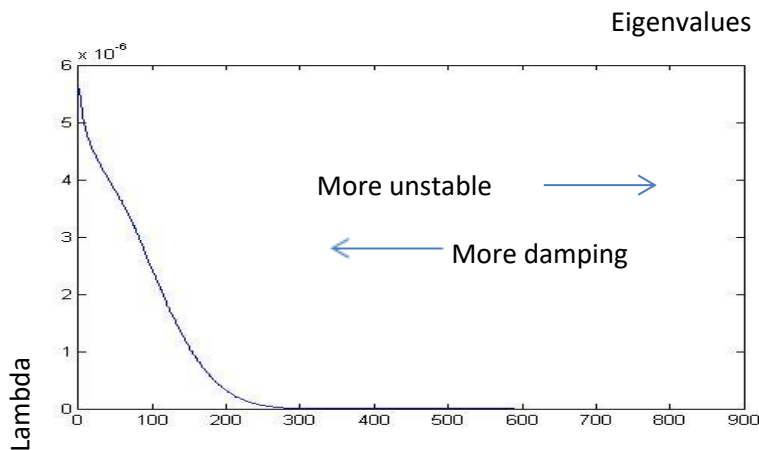


Fig.A.1 .Damping constant lambda as a function of the eigenvalues of $M^T * M$

We will choose lambda around $(NT/2)$ eigenvalue of the matrix $M^T * M$ to be able to use it in the inversion. The output reflectivity (r) will then depend on the value of lambda and introduce damping.

Fig.A.1 shows that when we choose smaller eigenvalues lambda will increase and r is more damped. When lambda increase we found that the effect of the inversion was less and over a threshold value no effect at all. When we increase eigenvalues, lambda decrease. Then we get less damping but r is also more unstable, and can introduce noise. For all calculations in our article we choose lambda=4.8.

It should be taken care to choose the right damping constant (λ) in order to perform the inversion. The choice must be related to noise level, choice of Butterworth filtering and scaling until one gets a satisfying result. We have not discussed this here, but plan to do it in future research.